



HAL
open science

Silver-Doped Hydroxyapatite Thin Layers Obtained by Sol-Gel Spin Coating Procedure

Alina Mihaela Prodan, Simona Liliana Iconaru, Mihai Valentin Predoi, Daniela Predoi, Mikael Motelica-Heino, Claudiu Stefan Turculet, Mircea Beuran

► **To cite this version:**

Alina Mihaela Prodan, Simona Liliana Iconaru, Mihai Valentin Predoi, Daniela Predoi, Mikael Motelica-Heino, et al.. Silver-Doped Hydroxyapatite Thin Layers Obtained by Sol-Gel Spin Coating Procedure. *Coatings*, 2020, 10 (1), pp.14. 10.3390/coatings10010014. insu-02426951

HAL Id: insu-02426951

<https://insu.hal.science/insu-02426951>

Submitted on 3 Jan 2020

HAL is a multi-disciplinary open access archive for the deposit and dissemination of scientific research documents, whether they are published or not. The documents may come from teaching and research institutions in France or abroad, or from public or private research centers.

L'archive ouverte pluridisciplinaire **HAL**, est destinée au dépôt et à la diffusion de documents scientifiques de niveau recherche, publiés ou non, émanant des établissements d'enseignement et de recherche français ou étrangers, des laboratoires publics ou privés.

Article

Silver-Doped Hydroxyapatite Thin Layers Obtained by Sol-Gel Spin Coating Procedure

Alina Mihaela Prodan ^{1,2}, Simona Liliana Iconaru ³, Mihai Valentin Predoi ⁴, Daniela Predoi ³, Mikael Motelica-Heino ⁵, Claudiu Stefan Turculeț ^{1,2} and Mircea Beuran ^{1,2,*}

¹ Carol Davila University of Medicine and Pharmacy, 8 Eroii Sanitari, Sector 5, 050474 Bucharest, Romania; prodan1084@gmail.com (A.M.P.); c.s.turculeț@gmail.com (C.S.T.)

² Emergency Hospital Floreasca Bucharest, 8 Calea Floresca, 014461 Bucharest, Romania

³ National Institute of Materials Physics, Atomistilor Street, No. 405A, P.O. Box MG 07, 077125 Magurele, Romania; simonaiconaru@gmail.com (S.L.I.); dpredoi@gmail.com (D.P.)

⁴ University Politehnica of Bucharest, BN 002, 313 Splaiul Independentei, Sector 6, 060042 Bucharest, Romania; predoi@gmail.com

⁵ ISTO, UMR 7327 CNRS Université d'Orléans, 1A rue de la Férollerie, 45071 Orléans CEDEX 2, France; mikael.motelica@univ-orleans.fr

* Correspondance: beuranmircea@gmail.com

Received: 27 November 2019; Accepted: 23 December 2019; Published: 25 December 2019

Abstract: The main objective of this paper is to develop silver-doped hydroxyapatite suspensions (HApAg) with different concentrations of silver ($x_{Ag} = 0.05$ and $x_{Ag} = 0.2$) in order to obtain uniform and homogenous layers by spin-coating procedure. The colloidal properties of HApAg suspensions are evaluated by dynamic light scattering (DLS) analysis, ζ -potential (ZP), and ultrasound measurements. The ultrasound studies show that the HApAg20 sample revealed better stability than the HApAg5 sample. The structural and morphological analysis on suspensions and thin layers is also conducted. It is observed that the particles of the two samples have a similar shape and are uniform. The layers obtained present a homogeneous appearance of the surface without evidence of cracks or interruption of the coatings. The in vitro antifungal studies conducted on the two thin layers at two different time intervals (24 and 48 h) show that both HApAg5 ($x_{Ag} = 0.05$) and HApAg20 ($x_{Ag} = 0.05$) nanoparticles suspensions and composite layers inhibit the development of colony forming units (CFU) even after 24 h of incubation comparative to the control, represented by the *Candida albicans* (*C. albicans*) culture in a proper medium. The fungicidal effect was evident after 48 h of incubation in the case of both HApAg20 nanoparticles suspensions and composite layers.

Keywords: silver; hydroxyapatite; suspension stability; sol-gel spin coating; antimicrobial properties

1. Introduction

In the last years, despite the great progress made in the medical field, due to the emergence of bacterial strains resistant to antibiotics, bacterial infections are still a serious threat and have a great influence on the morbidity, mortality, and medical costs of patients [1–3]. The risks of developing life-threatening bacterial infection are considered to be increased mostly in the implant-related medical field. The microorganisms that are found in the implanted biomaterials usually lead to post-implantation infections in the human body, which most often requires the removal of prosthesis in order to save the patient's life [4–6]. Infections caused by multi-resistant Gram-positive and Gram-negative organisms are usually treated by traditional systematic drug administration, in which drugs are absorbed into the bloodstream. These common practices have numerous drawbacks, the most important being the possible toxicity and also the low drug penetration into the target tissue.

Nevertheless, in implant surgery, the antimicrobial effects of the surgical site is also of outmost importance for the prevention of bacterial infection development. In this case, the administration of an antimicrobial agent at precisely the surgical site is an alternative therapeutic approach [6–9]. Regularly, both in orthopedics as well as in dentistry, the fixation of the implants with the surrounding tissue is directly related to the contact of the implant with the surrounding tissue. Implant failure is usually associated with the apparition of infection, which perturbs the natural healing process, making the implant loose as a result of the development of microbial colonies and biofilms on the implant's surface [10–13]. During the years, the mechanisms of the development of microbial colonization of the medical prosthesis at the time of implantation were attributed to the manipulation of tissue and implantation device and also to contaminated sterile implants [12]. It has been reported that from 1033 cases of total hip and total knee prosthetic arthroplasty, the majority of the implant-related infections were caused by aerobic cocci, most commonly *Staphylococcus aureus* (*S. aureus*), (23%) and coagulase-negative staphylococci (25%) [12]. Moreover, other important microbial strains involved in the development of post-operative implant-related infections are the *C. albicans* species [14]. Moreover, *C. albicans* is a common opportunistic fungal microbial strain that has the ability to colonize both human mucosal and biomaterial surfaces and its well-known for its capability of easily developing microbial biofilms, which are resistant to conventionally antimicrobial drugs [14]. In this context, the antimicrobial activity of the implant prosthesis has become an additional necessary prevention measure, in implant related medical interventions [13,15,16]. Nowadays, due to its extraordinary biocompatibility and osteoconductive properties, one of the most used biomaterials in bone tissue engineering is hydroxyapatite (HAp) even though on its own it exhibits no antimicrobial activity [17]. On the other hand, one of the oldest materials, well-known for its outstanding antimicrobial activity, is silver and silver ions. Silver and silver-based materials have been used since ancient times for wound disinfection and also in the treatment of microbial infections [18,19]. Recent studies have reported that silver ions could be successfully incorporated in the HAp structure [20–22], but there is scarce information regarding silver ion release in long-term studies and also regarding the development of stable materials for use as coatings for various medical devices [23]. Furthermore, studies have shown that, even in low concentrations, Ag^+ ions that are released from the silver doped hydroxyapatite (HAp/Ag) can ensure antibacterial effect, but when present in high concentrations they could become toxic [24,25]. Therefore, one of the biggest issues addressed today at a global scale is the obtaining of stable materials with both biocompatible and antimicrobial properties that could be used in the development of coatings for medical devices. During the years, hydroxyapatite-coated implants incorporated with antimicrobial agents were proposed as a solution for the prevention or treatment of implant-related infections, due to the fact that they could release antimicrobial agents to specific regions [25]. Therefore, this study focuses on the development of biocompatible stable solutions of silver-doped hydroxyapatite with antifungal properties for the preparation of coatings for biomedical devices.

In this paper, silver-doped hydroxyapatite with $x_{\text{Ag}} = 0.05$ (HApAg5) and $x_{\text{Ag}} = 0.2$ (HApAg20) samples, without impurities, are successfully synthesized by a sol-gel process. X-ray diffraction (XRD), transmission electron microscopy (TEM), and scanning electron microscopy (SEM) are employed to characterize the structure and morphology of HApAg5 and HApAg20 nanoparticles in suspensions. The colloidal properties are evaluated by dynamic light scattering (DLS) and zeta potential (ZP) analysis. In addition, the ultrasound measurement is used to evaluate the stability of HApAg5 and HApAg20 suspensions. The homogeneity and morphology of the thin layers obtained by spin-coating procedure are assessed by SEM. The antimicrobial studies are conducted on HApAg5 and HApAg20 suspensions and obtained layers.

2. Materials and Methods

2.1. Materials

The reagents, such as silver nitrate AgNO_3 , Alfa Aesar, Karlsruhe, Germany; 99.99% purity], ammonium hydrogen phosphate $[(\text{NH}_4)_2\text{HPO}_4]$, Alfa Aesar, Karlsruhe, Germany; 99.99% purity],

calcium nitrate [$\text{Ca}(\text{NO}_3)_2 \cdot 4\text{H}_2\text{O}$, Aldrich, St. Louis, MI, USA], and ethanol [$\text{C}_2\text{H}_5\text{OH}$] were used for the obtaining of silver-doped hydroxyapatite (HApAg) nanoparticles in suspension by sol-gel method in order to prepare the HApAg thin layers on Si substrate by spin-coating procedure.

2.2. Thin Layer of Silver-Doped Hydroxyapatite

Silver nitrate (AgNO_3), calcium nitrate ($\text{Ca}(\text{NO}_3)_2 \cdot 4\text{H}_2\text{O}$), and ammonium hydrogen phosphate ($(\text{NH}_4)_2\text{HPO}_4$) were used to obtain the $\text{Ca}_{10-x}\text{Ag}_x(\text{PO}_4)_6(\text{OH})_2$ gel, with $x_{\text{Ag}} = 0.05$ and $x_{\text{Ag}} = 0.2$. The gel obtained after the well-controlled steps was used for the preparation of the HApAg5 and HApAg20 thin layers. In the first step, $(\text{NH}_4)_2\text{HPO}_4$ was dissolved in ethanol and then stirred for 2 h at 40 °C. At the same time, $\text{Ca}(\text{NO}_3)_2 \cdot 4\text{H}_2\text{O}$ and (AgNO_3) were dissolved in ethanol and mixed for 2 h at 40 °C. The solution containing P was added dropwise to the solution containing Ca and Ag and stirred continuously. The resulting solution was stirred for 12 h at 100 °C [26]. The molar ratio $[\text{Ca} + \text{Ag}]/\text{P}$ was 1.67, while the pH value of the final solution was kept constant at 10. During synthesis, the pH was kept constantly equal to 10 by addition of NH_3 . The resulting final gel was placed in an ultrasound bath for 12 h. The final gel obtained was used to make HApAg layers on Si substrate by spin-coating procedure. To achieve the HApAg5 and HApAg20 layers, 0.5 mL of the final gel was used, which was placed, using a syringe, on the top of the Si substrate. The centrifugation time to obtain the coating was 60 s, while the speed was 2000 rpm. Both samples were obtained under the same conditions by coating the Si substrate repeatedly 35 times. After each coating, the samples were dried for 5 min at 60 °C. Finally, the HApAg5 ($x_{\text{Ag}} = 0.05$) and HApAg20 ($x_{\text{Ag}} = 0.2$) samples were heat treated at 700 °C for 4 h to remove solvents and to obtain crystalline structure layers.

2.3. Characterization Methods

The X-ray diffraction analysis of the HApAg5 and HApAg20 samples were registered using a Bruker D8 Advance diffractometer, with nickel filtered $\text{CuK}\alpha$ ($\lambda = 1.5418 \text{ \AA}$) radiation, and a high efficiency one-dimensional detector (Lynx Eye type). The diffraction patterns were recorded in the 2θ range 10° – 80° , with a step of 0.02° and 34 s measuring time per step.

The resulting HApAg5 and HApAg20 suspensions samples used to obtain the thin layers by spin-coating procedure on Si substrate were investigated by DLS analysis and ζ -potential (ZP) measurements. Dynamic light scattering (DLS) and ζ -potential were effectuated at 25 ± 1 °C using SZ-100 Nanoparticle Analyzer (Horiba-SAS France, Longjumeau, France). All the samples were diluted in water 10 times before DLS and ζ -potential measurements. Three determinations were registered for each sample and the final value was established by mediating the three measurements.

The samples were also investigated by transmission electron microscopy measurements using a CM 20 (Philips- FEI, Hillsboro, OR, USA) transmission electron microscope equipped with a Lab6 filament operating at 200 kV.

The morphology of the samples was investigated by SEM using a HITACHI S4500 microscope (Hitachi, Ltd., Tokyo, Japan). The 3D surface plots of the SEM images were obtained using Image J software (ImageJ 1.51j8, National Institutes of Health, Bethesda, MD, USA) [27].

For non-destructive ultrasound studies, a measurement system consisting of a thermo-controlled vessel, a pulser-receiver, an oscilloscope, and an H5K ultrasonic transducer (produced by General-Electric, Krautkramer, Germany), was used with 5 MHz central frequency and a very short pulse. The pulser-receiver device operates in the present work as a pulser-receiver mode on a single transducer that fulfills both roles. The device emits a short pulse (Dirac signal) of high voltage (300 V). The transducer produces a resonance signal and then receives the echoes from the measured liquid. The device amplifies these signals (adjustable amplification up to 100 dB) and applies them to the output terminal, which connects to the input of the oscilloscope. Bi-distilled water was used as the standard liquid. To reduce the electrical noise, the signals are mediated, in our case a signal is displayed after mediation of 32 acquired signals. For each fluid, the temperature of the respective liquid is measured with an accuracy of 0.1 °C before the ultrasonic analysis. With three signals available from the reference liquid (bi-distilled water) and from the suspension based on silver doped hydroxyapatite (HApAg) analyzed, the elaborated program determines the time difference between

the equivalent signals of the two liquids. Having three pairs of signals, an average will be made for the three-time differences. The time difference is used to calculate the speed of the ultrasonic waves through the analyzed liquid, thereby knowing precisely the speed of these waves through the reference liquid (bi-distilled water) and the distance traveled by the ultrasonic waves. This distance can be measured using two successive echoes through bi-distilled water, in which case the accuracy reaches 0.01 mm.

2.4. In Vitro Antifungal Assays

The antifungal properties of the HApAg5 and HApAg20 suspensions and thin layers were determined using a common reference strain of fungi, *Candida albicans* from the American Type Culture Collection (ATCC, Old Town Manassas, Virginia, USA), *Candida albicans* ATCC 10231. The assessment of the antifungal properties of the samples were performed using fungal suspensions of a known density ($\sim 1.5 \times 10^5$ – 10^6 colony forming units (CFU)/mL), obtained from 15 to 18 h fungal cultures as reported in Iconaru et al. [28]. The fungal biofilm development on the surface HApAg5 and HApAg20 thin layers was qualitatively investigated by scanning electron microscopy (SEM). For the SEM visualization, the HApAg5 and HApAg20 thin layers were incubated for 24 and 48 h with the *C. albicans* ATCC 10231 culture medium, removed from the medium after 24 and 48 h, and then washed with sterile saline solution. After being washed with sterile saline solution, the adherent fungal cells were fixed using cold methanol and prepared for scanning electron microscopy (SEM) visualization. The antifungal activity of HApAg5 and HApAg20 suspensions and thin layers was also evaluated by a quantitative assay. The quantitative assays of the antifungal properties of HApAg5 and HApAg20 suspensions and thin layers after 24 and 48 h was performed using an adapted method (E2149-10; ASTM International) [29,30] previously described in Predoi et al. [31]. The experiments were done in triplicate and the results were presented as mean \pm SD.

3. Results and Discussions

In order to evaluate the crystalline structure of the analyzed samples, XRD studies were performed on the powders obtained after the centrifugation of the HApAg5 and HApAg20 suspensions and drying of the resulting precipitate at 80 °C. The XRD pattern of the as synthesized HApAg5 and HApAg20 samples by sol-gel process and the standard model of HAp (JCPDS card No. 09-0432) are presented in Figure 1. As can be seen in Figure XRD, the main ten peaks of HApAg5 and HApAg20 samples that were identified at 25.88, 31.80, 32.2, 32.92, 34.5, 39.82, 46.70, 49.49, 53.12, and 64.10 can be assigned to the at (002), (211), (112), (300), (202), (310), (222), (213), (004), and (323) lattice planes of hexagonal HAp.

The crystalline size, D_{XRD} , of the synthesized HApAg5 and HApAg20 samples was estimated from the XRD pattern using the Debye–Scherrer formula [32,33]:

$$D_{\text{XRD}} = 0.9\lambda / B \cos \theta_{\text{hkl}} \quad (1)$$

where, D_{XRD} is the crystallite size, λ is the wavelength of the monochromatic X-ray beam, B is the full width at half maximum (FWHM) of the peak at the maximum intensity, and $\theta_{\text{(hkl)}}$ is the peak diffraction angle that satisfies Bragg's law for the (hkl) plane. To calculate the crystallite size, the (002) reflection peak from the XRD pattern was used. The D_{XRD} was estimated to have a mean value of 20.1 ± 2.7 nm for HApAg5 and 19.1 ± 1.3 nm for HApAg20.

In the XRD pattern of HApAg5 and HApAg20 samples no additional peaks could be observed that could be attributed to impurities. The lack of additional maximums shows that following the synthesis process, there are pure samples, without impurities. As established after XRD analysis, these samples were well crystallized and could be defined as Hap, seeing that all of the diffraction peaks coincide well with the standard HAp pattern.

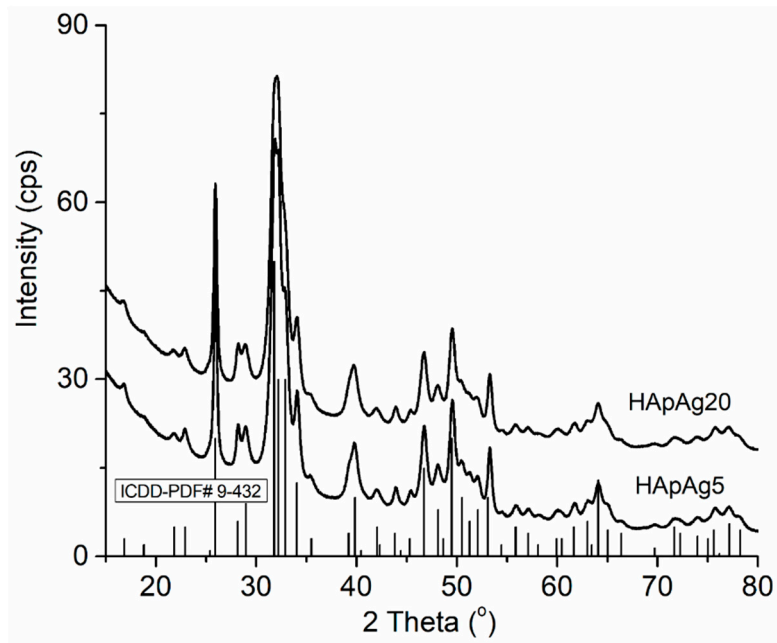


Figure 1. XRD pattern of the HApAg5 and HApAg20 samples and the standard pattern of the HAp (JCPDS card No. 09-0432).

The homogeneity and morphology of the HAp, HApAg5, and HApAg20 particles in suspension were evaluated by TEM and SEM. From the TEM and SEM images presented in Figure 2a–f, it was observed that the particles of the two samples have a similar shape and are uniform. The TEM and SEM investigations revealed that for the HApAg samples with $x_{Ag} = 0$, $x_{Ag} = 0.05$ and $x_{Ag} = 0.2$ samples, the particles are ellipsoidal in shape and are of the order of nanometers. The results of the two analyzes showed that the Ag⁺ doping has little influence on the shape and size of the nanoparticles. The average particle size for the HApAg5 sample deduced from the TEM was of 22.9 ± 3.5 nm, while for the HApAg20 sample it was 21 ± 1.7 nm. The size distribution from TEM images was obtained by counting approximately 700 particles. From the SEM studies, an average size equal to 22.3 ± 4.2 nm for the HApAg5 sample and 22.7 ± 3.2 nm for the HApAg20 sample was deduced. The results obtained from the TEM and SEM studies are in agreement with those obtained from the XRD studies.

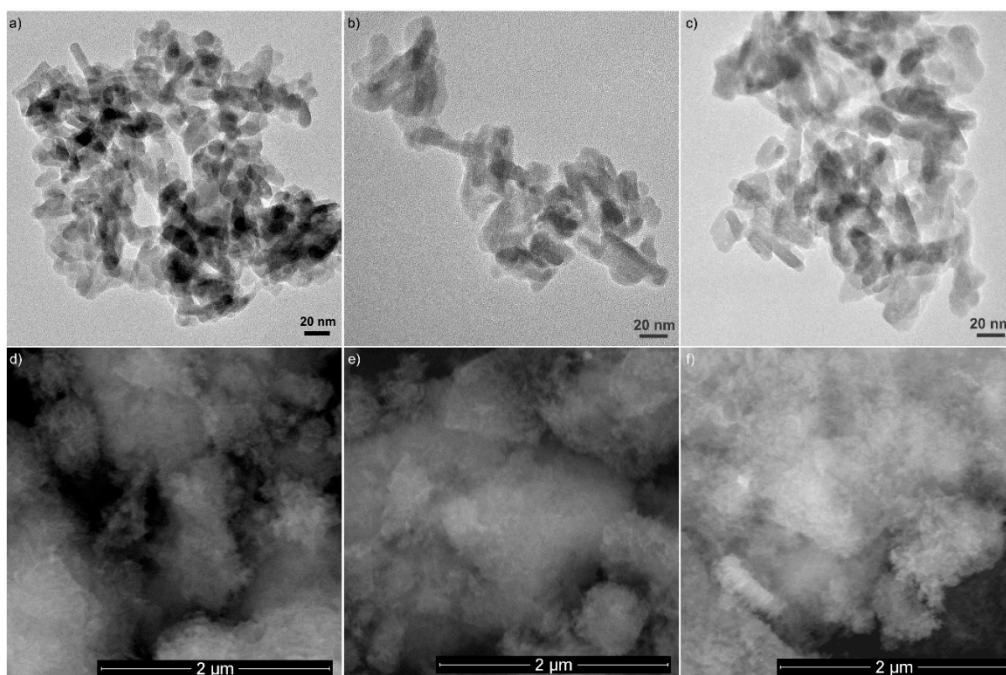


Figure 2. TEM micrographies and SEM images and of the HApAg samples with $x_{Ag} = 0$ (a,d), $x_{Ag} = 0.05$ (b,e) and $x_{Ag} = 0.2$ (c,f).

Important information regarding determining the hydrodynamic diameter of the nanoparticles but also the size distribution profile of the particle in suspension were evaluated by dynamic light scattering (DLS) analysis. The size distribution profiles of HApAg5 and HApAg20 nanoparticles in suspension are presented in Figure 3. The size distributions evaluated by DLS showed two peaks for the HApAg5 suspension suggesting that the sample present two populations (Figure 3a). The HApAg5 sample presents a bi-modal particle distribution with two population of particles in suspension of hydrodynamic diameter of 26.84 ± 2 nm and 57.36 ± 2 nm, respectively. The size distribution obtained by DLS presented a single peak for the HApAg20 sample, suggesting that the sample was mono-dispersed (Figure 3b). The hydrodynamic diameter of HApAg20 sample was estimated at 22.52 ± 1 nm. As can be seen, increasing the silver concentration decreases the hydrodynamic radius of particles, suggesting that the silver concentration is responsible for this effect. It is well-known that the stability estimation of the colloidal suspensions can be achieved using the zeta potential analysis. The zeta potential can play an important role in providing information regarding the behavior of suspensions. As shown in Figure 3c,d, the increase of silver concentration in silver doped hydroxyapatite suspensions from 5 wt% (HApAg5) to 20 wt% (HApAg20) causes the increase of the zeta potential of silver doped hydroxyapatite suspensions from -15.85 mV to -29.12 mV and leads to the increase of stability.

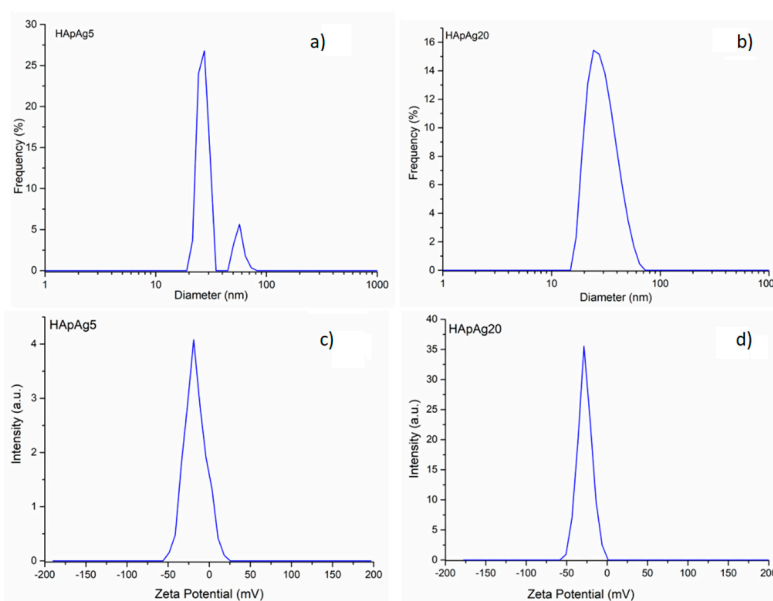


Figure 3. Size distribution of HApAg5 (a) and HApAg20 (b) suspensions measured by a dynamic light scattering method. Zeta potential for the HApAg5 (c) and HApAg20 (d) suspensions.

For a more accurate estimation of the stability of the solutions used in making coatings, ultrasound measurements were performed, as they provide us with information on the concentrated solutions made of nanoparticles in suspension.

The velocity of the ultrasonic waves through the analyzed liquid is a feature of it and can serve to characterize the possible deviations from the concentration in the case of the preparation of other samples of the same type. The frequency spectrum of each echo through the analyzed liquid can be measured and normalized to the echo obtained through the reference fluid. Thus, maxima are obtained in the range of interest (in the range 0.5–7.5 MHz) for the 5 MHz transducer, which represent resonances of the suspended particles. The first three echoes for the reference liquid (bi-distilled water), HApAg5 and HApAg20 samples at 5 MHz, are shown in Figure 4. The spectral amplitudes of HApAg5 and HApAg20 relative to those of the reference liquid are shown in Figure 5. Following these measurements, an analysis

could be made according to the frequency of the signals acquired for the two analyzed samples. The elastic properties of the nanoparticles in suspension were highlighted by the ratio of the spectral amplitudes at each of the analyzed frequencies in the central frequency band on the translator frequency. For the two samples analyzed, three resonance frequencies at 1.1, 5.1, and 6.9 MHz were highlighted (Figure 5). The amplitude ratio to the reference fluid in the case of HApAg5 sample is more than three times at 1.1 MHz reaching 5.5 to 5.1 MHz and below four at 6.9 MHz (Figure 5a). This increase is due to the presence of silver doped hydroxyapatite nanoparticles suspended in bi-distilled water. In the case of the HApAg20 sample, at the same frequencies of 1.1, 5.1, and 6.9 MHz, the relative amplitudes increased to 4.7, 7.5, and 10 (Figure 5b). An increase in resonance maxima in the HApAg20 sample compared to HApAg5 may be due to an increase in the silver concentration in the sample from $x_{Ag} = 0.05$ to $x_{Ag} = 0.2$. The speed of the ultrasound waves through the two samples was also measured. The average speed on the three echoes in the HApAg5 suspension was equal to 1486.78 ± 1.03 m/s. In the HApAg20 suspension the mediated velocity was equal to 1484.12 ± 1.55 m/s while in the reference fluid it was equal to 1492.07 m/s. A decrease of the mediated speed for HApAg5 and HApAg20 samples is given by the porosity, density, and compressibility of the silver-doped hydroxyapatite nanoparticles. As it can be seen, the concentration of silver plays a very important role in the speed of ultrasonic waves. Based on the measured data and taking into account the density of the liquid (with suspended particles), it was possible to determine the elastic compressibility constant (K) for both the analyzed samples (HApAg5 and HApAg20) as well as for the reference fluid. For the HApAg5 sample, a value identical to that of water (2.226 MPa) was obtained, while for the HApAg20 sample the value of the elastic compressibility constant was equal to 2.593 MPa.

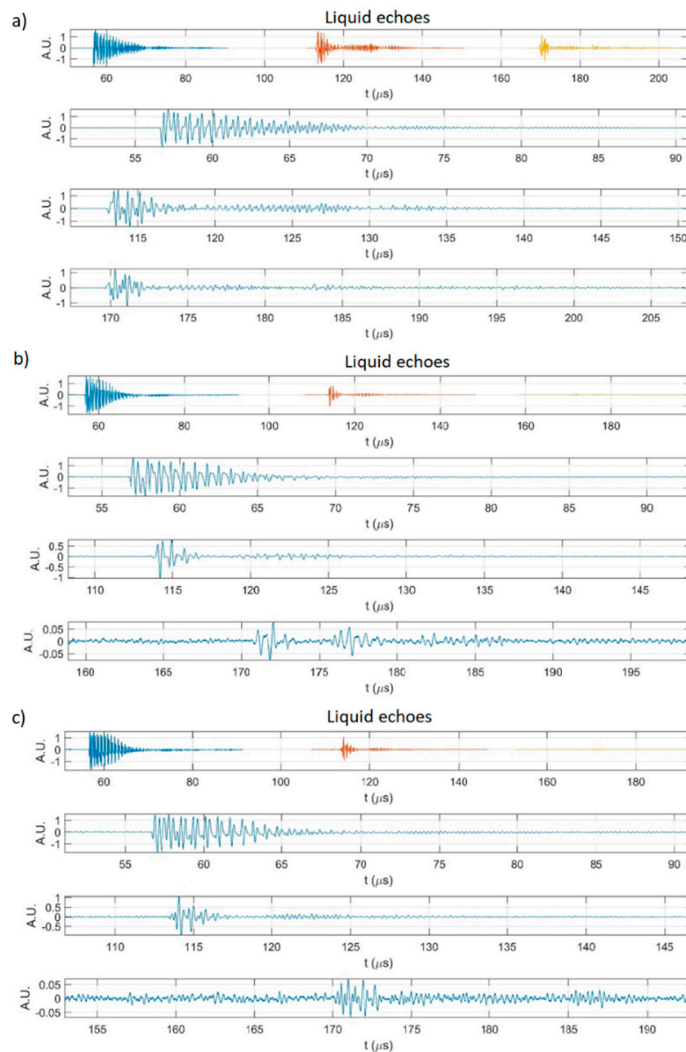


Figure 4. The first three echoes for the reference liquid (a) HApAg5 (b), HApAg20 (c), at 5 MHz grouped (top) and separated in the following three windows of the figure.

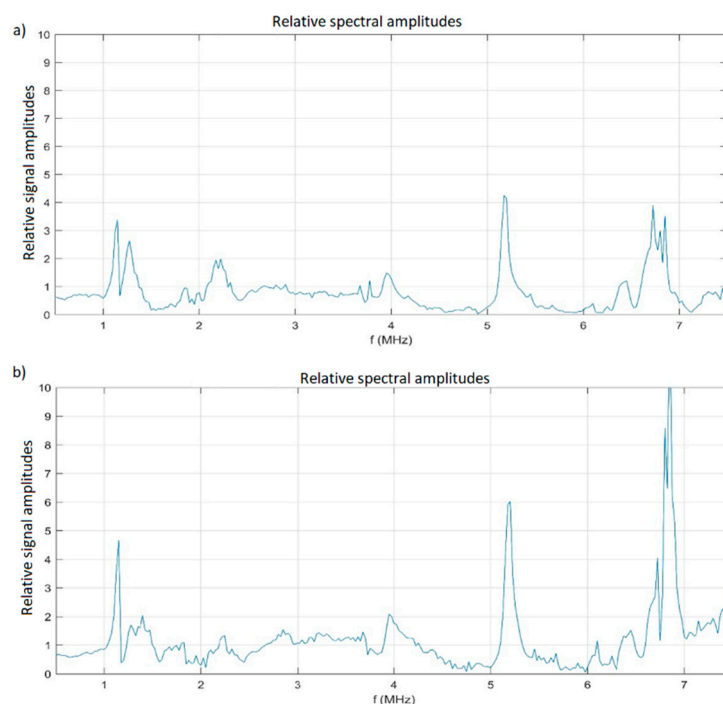


Figure 5. Spectral amplitudes of HApAg5 (a) and HApAg20 (b) relative to those of the reference liquid, for the first echo.

Another very important measured parameter was the attenuation. The attenuation measured in the reference fluid was equal to 3.35198 Np/m, while for the HApAg5 and HApAg20 samples it was 7.28932 Np/m and 6.8176 Np/m, respectively. It is observed that the attenuation of the signal amplitude decreases in the case of the HApAg20 sample compared to HApAg5, which shows that the attenuation is closely related to the particle size, porosity, and concentration of nanoparticles in the analyzed suspension as well as their stability. The stability of the measured samples can be correlated with the value of the attenuation and is good for an attenuation close to that of the water. Following these studies, we can say that the HApAg20 sample shows better stability than the HApAg5 sample. This behavior could be due to the size of the particles in suspension, which are smaller for the HApAg20 sample ($D_{\text{XRD}} = 19.1 \pm 0.8$ nm) than for the HApAg5 sample ($D_{\text{XRD}} = 20.1 \pm 1.3$ nm).

The surface morphology of the HApAg5 and HApAg20 composite layers was investigated using SEM analysis. SEM micrographs of the composite coatings images are presented in Figure 6a,b. The results of the SEM investigations revealed a homogenous aspect of the surface of both investigated samples. There was no evidence of fissures or discontinuities of the coatings on the surface areas presented in the SEM images. Moreover, even though the SEM analysis revealed that both HApAg5 and HApAg20 composite layers presented a homogeneous structure, it can be observed that there is a difference in the morphology of the two samples. The SEM micrograph of the HApAg5 composite layers exhibits smaller grains and a denser structure compared to that of the HApAg20 composite layers. These differences are due to the fact that the concentration of silver ions in the HAp matrix has a small impact on the particle size. Furthermore, the SEM micrographs also revealed that the coatings are composed of round rod-like shaped particles having nanometric sizes.

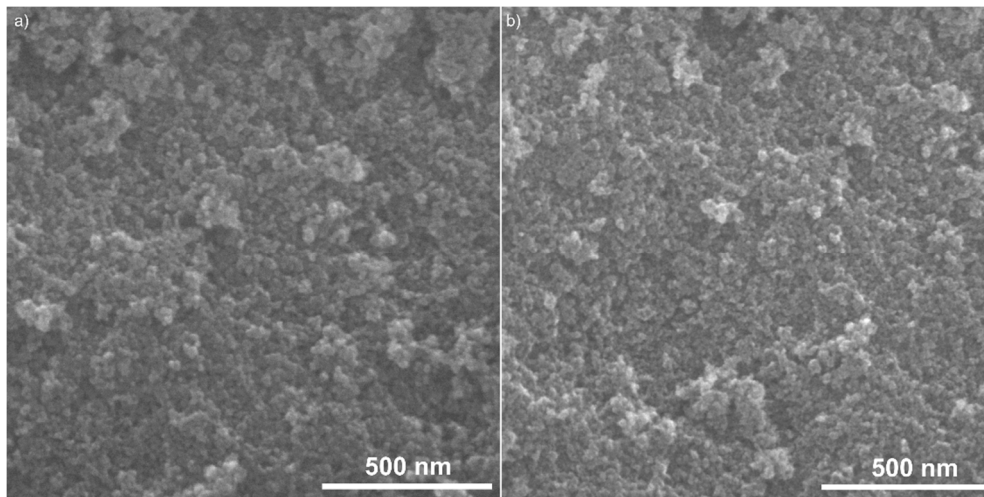


Figure 6. SEM images of the HApAg20 (a) and HApAg5 (b) composite layers.

In the medical field, *Candida albicans* is defined as an opportunistic fungus, due to the fact that it usually affects disease-immunocompromised patients or people whose natural flora have been altered from various reasons, and it is also classified as being the most prevalent cause of fungal infections. In recent years, despite the progress made in the pharmacology field, and the development of potent antibiotics and other antimicrobial means, infections caused by the microorganism are still a major cause in morbidity and mortality everywhere, due to the apparition of multidrug-resistant microbial strains and biofilm associated infections [34,35]. Therefore, in this study the HApAg5 and HApAg20 composite layers were investigated for their efficiency against the development of *C. albicans* ATCC 10231 fungal cells on their surfaces, as well as for their capability of preventing biofilm formation. The antifungal activity of HApAg5 and HApAg20 nanoparticles suspensions and composite layers was investigated using the reference fungal strain *C. albicans* ATCC 10231. The results of the in vitro antifungal assays were presented in Figure 7. The in vitro antifungal studies were conducted at two different time intervals (24 and 48 h) using an adapted method for testing the antimicrobial activity under dynamic contact conditions. The quantitative assays highlighted that both HApAg5 and HApAg20 nanoparticles suspensions and composite layers inhibited the development of colony forming units (CFU) even after 24 h of incubation comparative to the control, represented by the *C. albicans* culture in a proper medium.

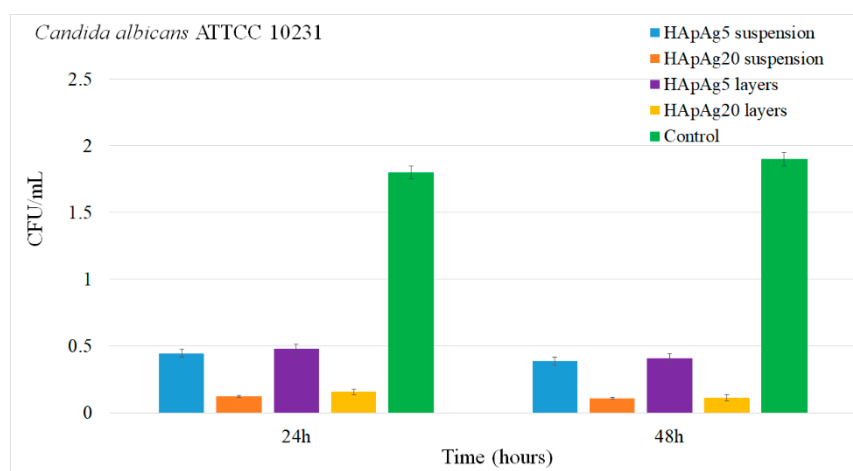


Figure 7. Antifungal activity of HApAg5 and HApAg20 nanoparticles suspension and composite layers against fungal strain *C. albicans* ATCC 10231.

The results of the in vitro antifungal assay highlighted that the inhibitory effect against the development of *C. albicans* CFU was more pronounced in the case of HApAg5 and HApAg20

nanoparticles suspensions that in the case of HApAg5 and HApAg20 composite layers. Furthermore, it can be seen that the inhibitory effect of the samples against the development of *C. albicans* CFU was strongly influenced by the incubation time. In the case of both HApAg20 nanoparticle suspensions and composite layers, after 48 h of incubation, the *C. albicans* cells development had values significantly smaller related to the ones of the control, suggesting a fungicidal effect. This behavior has been attributed to the presence of silver ions in the suspensions and composite layers and to their controlled released in time. A significant inhibitory effect against the development of *C. albicans* was also noticed after 24 h of incubation for all the investigated samples. In addition, the results of the antifungal assays have also emphasized that the HApAg nanoparticle suspensions exhibited a better antifungal activity against *C. albicans* cells regardless of the incubation time.

The results obtained in this study are in accord with previously reported studies regarding the potential antimicrobial properties of materials and composite layers based on hydroxyapatite enhanced with various antimicrobial agents, such as metal ions, that are known to possess antimicrobial properties [36–38]. Despite the progress made in the biomedical field, several studies have reported that the development of implant-related infection is still of great concern and that *C. albicans* can easily colonize and aggregate on prostheses and implants [39–41]. In this context, studies regarding the development, adhesion, and biofilm formation of fungal cells on the surfaces of materials that are currently envisaged for the development of implantable devices that could lead to preventing or treating microbial infections are of great interest for the medical field.

The adherence of *C. albicans* fungal cells after 24 and 48 h of incubation on the surface of the HApAg5 and HApAg20 composite layers was studied using scanning electron microscopy (SEM). The result of the SEM visualization of the HApAg5 and HApAg20 composite layers exposed to *C. albicans* microbial culture for 24 and 48 h are presented in Figure 8a–d.

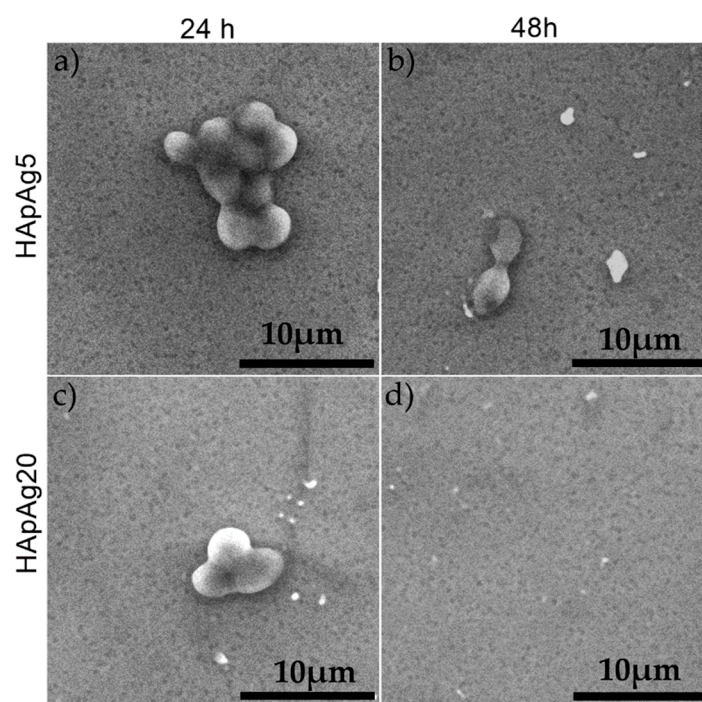


Figure 8. SEM images of *Candida albicans* ATCC 10231 cell development on HApAg5 composite layers after 24 and 48 h (a,b) and SEM images of *Candida albicans* ATCC 10231 cell development on HApAg20 composite layers after 24 and 48 h of incubation (c,d).

The results of the SEM investigations revealed that the morphology of the investigated cells were characteristic to *C. albicans*, exhibiting an ovaloid shape and having sizes ranging from 2.68 to 4.05 μm , dimensions specific to *C. albicans* fungal cells. Furthermore, the qualitative SEM investigations revealed that both tested HApAg thin layers significantly inhibited the fungal cells development even after 24 h (Figure 8a,c). Moreover, the images demonstrated that both HApAg5 and HApAg20

composite layers prevented the biofilm formation on their surfaces for both tested time intervals (Figure 8). In addition, the SEM images clearly emphasized that after 48 h of incubation (Figure 8d), the HApAg20 composite layers have completely eradicated the *C. albicans* fungal cells. A very strong inhibitory effect against the development and proliferation of *C. albicans* fungal cells was also observed in the case of HApAg5 composite layers after 48 h of incubation. The results of the SEM visualization are in agreement with the quantitative antifungal assays and highlighted that even though both HApAg composite layers exhibited strong antifungal activity, excellent results were obtained in the case of HApAg20 composite layers which managed to completely eliminate the *C. albicans* fungal cells.

It is well known that colloidal systems have a biological significance, especially since we know that all vital processes are colloidal in nature. The colloids category includes: blood, cell membranes, nerve fibers, and so forth. We know that, like any heterogeneous system, colloidal solutions are subject to phenomena of instability (sedimentation, flocculation, coacervation, coagulation) in the presence of electrolytes, non-electrolytes, and other macromolecules or insolvents. Furthermore, the pharmacological action of a drug substance may be influenced by the colloidal state. Thus, antiseptic action, as well as tolerability, are higher when we talk about stable colloidal systems. Thus, in this research, we highlighted the stability of the gels prepared both by ultrasound measurements and zeta potential measurements. Both the studies performed by ultrasound and zeta potential measurements showed that the stability of the obtained gels was better when the concentration of silver was increased. In addition to the silver concentration in the sample, the synthesis parameters also played an important role. Thus, by placing in an ultrasonic bath the final gel for 12 h, its stability increased. The results presented in this study were sustained by previously reported studies [36–38], which state that hydroxyapatite could be enriched with various metal ions in order to exhibit antimicrobial properties. Nonetheless, this study emphasizes for the first time the obtaining of stable AgHAp solutions with antimicrobial properties, using an adapted synthesis method, for the development of new and improved coatings on the basis of silver-doped hydroxyapatite. The results presented in this study are of great interest and establish that the antimicrobial properties of AgHAp coatings are strongly influenced by both the silver ion concentrations and the solution stability. The results of the antifungal in vitro assays obtained for the investigated samples are in good agreement with previously studies of the authors [21,22,42–44], having reported excellent antimicrobial properties of thin layers obtained from silver-doped hydroxyapatite powders or suspensions. Moreover, the results are also in good agreement with other existing studies that proved that, composite layers based on hydroxyapatite and silver ions are a promising tool for creating an antifungal agent for biomedical applications. In addition to previously reported studies, the results of this paper emphasize the obtaining of AgHAp coatings from the stable suspension of AgHAp synthesized by an adapted method. In addition to that, in the present study, the results highlighted that the antifungal properties of the AgHAp coatings obtained from stable AgHAp solutions with different silver ions concentrations were greatly influenced by the silver ion concentration and the time of incubation with the microbial cultures. Therefore, the best results were achieved in the case of AgHAp20 layers after 48 h of incubation with *C. albicans* fungal cells. These results have demonstrated that the fungicidal effect of AgHAp layers in the case of *C. albicans* strain was observed after 48 h of incubation even though a strong inhibitory effect on its development was noticed only after 24 h of incubation. The results clearly suggest that the AgHAp20 layers were more efficient in suppressing the development of *C. albicans* ATCC 10231 fungal cells. Furthermore, following the antifungal results, it has been observed that both AgHAp layers completely inhibited the biofilm formation of the *C. albicans* ATCC 10231.

4. Conclusions

The HApAg5 and HApAg20 composite layers were obtained by spin-coating procedure using silver-doped hydroxyapatite suspensions with $x_{Ag} = 0.05$ and $x_{Ag} = 0.2$ synthesized by sol-gel. The structural and morphological properties of the HApAg5 and HAp20 particle suspensions were evaluated by XRD, SEM, and TEM analysis. The colloidal properties of the suspensions were

evaluated by DLS and ZP analysis and their stability was investigated using ultrasound measurements. From the XRD results, the estimated D_{XRD} was 20.1 ± 2.7 nm for HApAg5 and 19.1 ± 1.3 nm for HApAg20. Moreover, the DLS analysis revealed a hydrodynamic diameter of 26.84 ± 2 nm in the case of HApAg5 and 57.36 ± 2 nm in the case of HApAg20. The stability of the HApAg5 and HApAg20 was also evidenced by the ZP studies and the ultrasonic measurements. Furthermore, SEM investigations of the HApAg5 and HApAg20 composite layers revealed a homogenous aspect of the surface of the samples that presented no fissures or discontinuities. The antimicrobial assays demonstrated that both HApAg5 and HApAg20 suspensions and composite layers exhibited a very good antifungal activity against *Candida albicans* ATCC 10231 cell development. Moreover, the results emphasize that HApAg5 and HApAg20 composite layers had a significant contribution in preventing the biofilm formation on their surfaces after 24 and 48 h of incubation. Furthermore, the antifungal results reveal that AgHAp20 composite layers exhibited a fungicidal effect on the *C. albicans* ATCC 10231 cell development after 48 h of incubation, making them better antifungal agents than AgHAp5 composite layers. Considering the fact that the majority of hospital and implant related infections are attributed to the *C. albicans* species, these results could have a great contribution to the development of novel composite coatings with antifungal properties.

Author Contributions: Conceptualization, D.P. and M.V.P.; methodology, D.P.; software, M.V.P.; validation, D.P., M.S.M-H. and M.V.P, M.B.; formal analysis, D.P., S.L.I, M.V.P, A.M.P., M.S.M-H.; investigation, D.P., S.L.I, M.V.P., C.S.T., A.M.P.; resources, D.P., S.L.I, M.V.P, M.S.M-H., M.B., A.M.P.; data curation, D.P., S.L.I and M.V.P; writing—original draft preparation, D.P., S.L.I, M.V.P, M.S.M-H.; writing—review and editing, D.P., S.L.I, and M.V.P.; visualization, D.P., S.L.I, M.V.P, M.S.M-H.; supervision, M.V.P, M.S.M.H.; project administration, A.M.P. and M.B.; funding acquisition, M.B., A.M.P., C.S.T.

Funding: This research was partially funded by the Romanian Ministry of Research and Innovation with the grant number and project number PN-III-P1-1.2-PCCDI-2017-0629/contract no. 43PCCDI/2018.

Acknowledgments: We thank A. Richard and A. Sauldubois from the “Centre de Microscopie Electronique” of the University of Orléans for assistance in SEM and TEM data acquisition. This work was supported by a grant of the Romanian Ministry of Research and Innovation, PCCDI-UEFISCDI, project number PN-III-P1-1.2-PCCDI-2017-0629/contract no. 43PCCDI/2018”.

Conflicts of Interest: The authors declare no conflict of interest.

References

1. Zhou, K.; Dong, C.; Zhang, X.; Shi, L.; Chen, Z.; Xu, Y.; Cai, H. Preparation and characterization of nanosilver-doped porous hydroxyapatite scaffolds. *Ceram. Int.* **2015**, *41*, 1671–1676.
2. Bai, X.; More, K.; Rouleau, C.M.; Rabiei, A. Functionally graded hydroxyapatite coatings doped with antibacterial components. *Acta Biomater.* **2010**, *6*, 2264–2273.
3. Rai, M.; Yadav, A.; Gade, A. Silver nanoparticles as a new generation of antimicrobials. *Biotechnol. Adv.* **2009**, *27*, 76–83.
4. Huang, Y.; Wang, W.; Zhang, X.; Liua, X.; Xua, Z.; Hanb, S.; Suc, Z.; Liuc, H.; Gaod, Y.; Yange, H. A prospective material for orthopedic applications: Ti substrates coated with a composite coating of a titania-nanotubes layer and a silver-manganesedoped hydroxyapatite layer. *Ceram. Int.* **2018**, *44*, 5528–5542.
5. Surmeneva, M.A.; Sharonova, A.A.; Chernousova, S.; Prymak, O.; Loza, K.; Tkachev, M.S. Incorporation of silver nanoparticles into magnetron-sputtered calcium phosphate layers on titanium as an antibacterial coating. *Colloid Surf. B* **2017**, *156*, 104–113, doi:10.1016/j.colsurfb.2017.05.016.
6. Kato, Y.; Ozawa, S.; Miyamoto, C.; Maehata, Y.; Suzuki, A.; Maeda, T.; Baba, Y. Acidic extracellular microenvironment and cancer. *Cancer Cell Int.* **2013**, *13*, 89.
7. Dubnika, A.; Loca, D.; Rudovica, V.; Parekh, M.B. Berzina-Cimdina, L. Functionalized silver doped hydroxyapatite scaffolds for controlled simultaneous silver ion and drug delivery. *Ceram. Int.* **2017**, *43*, 3698–3705.
8. Baradari, H.; Damia, C.; Dutreih-Colas, M.; Laborde, E.; Pecout, N.; Champion, E.; Chulia, D.; Viana, M. Calcium phosphate porous pellets as drug delivery systems: Effect of drug carrier composition on drug loading and in vitro release. *J. Eur. Ceram. Soc.* **2012**, *32*, 2679–2690.

9. Rauschmann, M.A.; Wichelhaus, T.A.; Stinal, V.; Dingeldein, E.; Zichner, L.; Schnettler, R.; Alt, V. Nanocrystalline hydroxyapatite and calcium sulphate as biodegradable composite carrier material for local delivery of antibiotics in bone infections. *Biomaterials* **2005**, *26*, 2677–2684.
10. Mack, D.; Rohde, H.; Harris, L.G.; Davies, A.P.; Horstkotte, M.A.; Knobloch, J.K.-M. Biofilm Formation in Medical Device-Related Infection. *Int. J. Artif. Organs.* **2006**, *29*, 343–359. doi.org/10.1177/039139880602900404.
11. Vaudaux, P.E.; Daniel, P.L.; Waldvogel, F.A. Host factors predisposing to and influencing therapy of foreign body infections. In *Infections Associated with Indwelling Medical Devices*; Bisno, A.L., Waldvogel, F.A., Eds.; ASM Press: Washington, DC, USA, 1994.
12. Steckelberg, J.M.; Osmon, D.R. Prosthetic joint infections. In *Infections Associated with Indwelling Medical Devices*; Bisno, A.L., Waldvogel, F.A., Eds.; ASM Press: Washington, DC, USA, 1994; pp. 1–436.
13. Shirkhazadeh, M.; Azadegan, M.; Liu, G.Q. Bioactive delivery systems for the slow-release of antibiotics—Incorporation of Ag⁺ ions into micro-porous hydroxyapatite coatings. *Mater. Lett.* **1995**, *24*, 7–12.
14. Williams, D.W.; Jordan, R.P.; Wei, X.Q.; Alves, C.T.; Wise, M.P.; Wilson, M.J.; Lewis, M.A. Interactions of *Candida albicans* with host epithelial surfaces. *J. Oral Microbiol.* **2013**, *5*, doi:10.3402/jom.v5i0.22434.
15. Ciobanu, G.; Ilisei, S.; Luca, C. Hydroxyapatite–silver nanoparticles coatings on porous polyurethane scaffold. *Mater. Sci. Eng. C Mater. Biol. Appl.* **2014**, *35*, 36–42.
16. Campoccia, D.; Montanaro, L.; Arciola, C.R. The significance of infection related to orthopedic devices and issues of antibiotic resistance. *Biomaterials* **2006**, *27*, 2331–2339.
17. Liu, X.M.; Mou, Y.A.; Wu, S.L.; Man, H.C. Synthesis of silver-incorporated hydroxyapatite nanocomposites for antimicrobial implant coatings. *Appl. Surf. Sci.* **2013**, *273*, 748–757.
18. Ciobanu, C.S.; Iconaru, S.L.; Pasuk, I.; Vasile, B.S.; Lupu, A.R.; Hermenean, A.; Dinischiotu, A.; Predoi, D. Structural properties of silver doped hydroxyapatite and their biocompatibility. *Mater. Sci. Eng. C Mater.* **2013**, *33*, 1395–1402.
19. Stanic, V.; Dimitrijević, S.; Tanasković, S.B.; Mitrić, M.; Pavlović, M.S.; Krstić, A.; Jovanović, D.; Raičević, S.; Janačković, D. Synthesis of antimicrobial monophasic silver-doped hydroxyapatite nanopowders for bone tissue engineering. *Appl. Surf. Sci.* **2011**, *257*, 4510–4518.
20. Costescu, A.; Ciobanu, C.S.; Iconaru, S.L.; Ghita, R.V.; Chifiriuc, M.C.; Marutescu, L.G.; Predoi, D. Fabrication, characterization, and antimicrobial activity, evaluation of low silver concentrations in silver-doped hydroxyapatite nanoparticles. *J. Nanomater.* **2013**, *2013*, 5.
21. Iconaru, S.L.; Chapon, P.; Le Coustumer, P.; Predoi, D. Antimicrobial activity of thin solid films of silver doped hydroxyapatite prepared by sol-gel method. *Sci. World J.* **2014**, *2014*, doi:10.1155/2014/165351.
22. Predoi, D.; Iconaru, S.L.; Predoi, M.V. Bioceramic Layers with Antifungal Properties. *Coatings* **2018**, *8*, 276.
23. McGonigle, E.J.; Webster, T.J.; Bhardwaj, G. Biocompatibility and Medical Device Coatings. In *Medical Coatings and Deposition Technologies*. Glocker, D.A.; Ranade, S.V., Eds.; John Wiley & Sons: Hoboken, NJ, USA, 2016, 131–180.
24. Singh, B.; Kumar, S.; Saha, N.; Basu, B.; Gupta, R.; Dubey, A.K. In vitro biocompatibility and antimicrobial activity of wet chemically prepared Ca_{10-x}Ag_x(PO₄)₆(OH)₂ (0.0 ≤ x ≤ 0.5) hydroxyapatites. *Mater. Sci. Eng. C Mater.* **2011**, *31*, 1320–1329.
25. Rameshbabu, N.; Sampath Kumar, T.S.; Prabhakar, T.G.; Sastry, V.S.; Murty, K.V.; Prasad Rao, K. Antibacterial nanosized silver substituted hydroxyapatite: Synthesis and characterization. *J. Biomed. Mater. Res. A* **2007**, *80*, 581–591.
26. Ciobanu, C.S.; Massuyeau, F.; Constantin, L.V.; Predoi, D. Structural and physical properties of antibacterial Ag-doped nano-hydroxyapatite synthesized at 100 °C. *Nanoscale Res. Lett.* **2011**, *6*, 613.
27. ImageJ Website. Available online: <http://imagej.nih.gov/ij> (accessed on 10 January 2018).
28. Iconaru, S.L.; Prodan, A.M.; Turculeț, C.S.; Beuran, M.; Ghita, R.V.; Costescu, A.; Groza, A.; Chifiriuc, M.C.; Chapon, P.; Gaiaschi, S.; et al. Enamel Based Composite Layers Deposited on Titanium Substrate with Antifungal Activity. *J. Spectrosc.* **2016**, *2016*, doi:10.1155/2016/4361051.
29. ASTM International. *ASTM E2149–13a Standard Test Method for Determining the Antimicrobial Activity of Antimicrobial Agents under Dynamic Contact Conditions*; ASTM International: West Conshohocken, PA, USA, 2013.
30. Fuchs, A.V.; Ritz, S.; Pütz, S.; Mailänder, V.; Landfester, K.; Ziener, U. Bioinspired phosphorylcholine containing polymer films with silver nanoparticles combining antifouling and antibacterial properties. *Biomater. Sci.* **2013**, *1*, 470–477.

31. Predoi, D.; Iconaru, S.L.; Predoi, M.V.; Buton, N.; Motelica-Heino, M. Zinc Doped Hydroxyapatite Thin Films Prepared by Sol–Gel Spin Coating Procedure. *Coatings* **2019**, *9*, 156.
32. Klug, H.P.; Alexander, L.E. *X-ray Diffraction Procedures for Polycrystallite and Amorphous Materials*, 2nd ed.; Wiley: New York, NY, USA, 1974.
33. Barrett, C.S.; Cohen, J.B.; Faber, J.; Jenkins, R.; Leyden, D.E.; Russ, J.C.; Predecki, P.K. *Advances in X-ray Analysis*; Plenum Press: New York, NY, USA, 1986; Volume 29.
34. Sipsasa, N.V.; Kontoyiannis, D.P. Invasive fungal infections in patients with cancer in the intensive care unit. *Int. J. Antimicrob. Agents* **2012**, *39*, doi:10.1016/j.ijantimicag.2011.11.017.
35. Chow, J.K.; Golan, Y.; Ruthazer, R.; Karchmer, A.W.; Carmeli, Y.; Lichtenberg, D.A.; Chawla, V.; Young, J.A.; Hadley, S. Risk factors for albicans and non-albicans candidemia in the intensive care unit. *Crit. Care Med.* **2008**, *36*, 1993–1998.
36. Predoi, D.; Iconaru, S.L.; Predoi, M.V.; Stan, G.E.; Buton, N. Synthesis, Characterization, and Antimicrobial Activity of Magnesium-Doped Hydroxyapatite Suspensions. *Nanomaterials* **2019**, *9*, 1295.
37. Predoi, D.; Iconaru, S.L.; Predoi, M.V.; Motelica-Heino, M.; Guegan, R.; Buton, N. Evaluation of Antibacterial Activity of Zinc-Doped Hydroxyapatite Colloids and Dispersion Stability Using Ultrasounds. *Nanomaterials* **2019**, *9*, 515.
38. Miranda, M.; Fernandez, A.; Lopez-Esteban, S.; Malpartida, F.; Moya, J.S.; Torrecillas, R. Ceramic/metal biocidal nanocomposites for bone-related applications. *J. Mater. Sci.* **2012**, *27*, 1655–1622.
39. Tobudic, S.; Kratzer, C.; Lassnigg, A.; Presterl, E. Antifungal susceptibility of *Candida albicans* in biofilms. *Mycoses* **2012**, *55*, 199–204.
40. Penk, A.; Pittrow, L. Role of fluconazole in the long-term suppressive therapy of fungal infections in patients with artificial implants. *Mycoses* **1999**, *42*, 91–96.
41. Ramage, G.; Martinez, J.P.; Lopez-Ribot, J.L. *Candida* biofilms on implanted biomaterials: A clinically significant problem. *FEMS Yeast Res.* **2006**, *6*, 979–986.
42. Ciobanu, C.S.; Groza, A.; Iconaru, S.L.; Popa, C.L.; Chapon, P.; Chifiriuc, M.C.; Hristu, R.; Stanciu, G.A.; Negrila, C.C.; Ghita, R.V.; et al. Antimicrobial activity evaluation on silver doped hydroxyapatite/polydimethylsiloxane composite layer. *BioMed Res. Int.* **2015**, *2015*, doi:10.1155/2015/926513.
43. Groza, A.; Ciobanu, C.S.; Popa, C.L.; Iconaru, S.L.; Chapon, P.; Luculescu, C.; Ganciu, M.; Predoi, D. Structural Properties and Antifungal Activity against *Candida albicans* Biofilm of Different Composite Layers Based on Ag/Zn Doped Hydroxyapatite-Polydimethylsiloxanes. *Polymers* **2016**, *8*, 131.
44. Iconaru, S.L.; Chifiriuc, M.C.; Groza, A. Structural and Antimicrobial Evaluation of Silver Doped Hydroxyapatite-Polydimethylsiloxane Thin Layers. *J. Nanomater.* **2017**, *2017*, 7492515.

